Performance Evaluation of Full-Duplex IAB Multi-Cell and Multi-User Network for FR2 Band

IEEE Access
Multidisciplinary ⋮ Rapid Review ⋮ Open Access Journal

Received May 3, 2021, accepted May 11, 2021, date of publication May 14, 2021, date of current version May 21, 2021.

Digital Object Identifier 10.1109/ACCESS.2021.3080307

Performance Evaluation of Full-Duplex IAB Multi-Cell and Multi-User Network for FR2 Band

A. BISHNU[1], (Member, IEEE), M. HOLM[2], (Member, IEEE), AND T. RATNARAJAH[1], (Senior Member, IEEE)

[1]Institute for Digital Communications, School of Engineering, The University of Edinburgh, Edinburgh EH8 9YL, U.K.
[2]Department of Radio Basestation Systems, Huawei Technologies Sweden AB, 164 40 Stockholm, Sweden

Corresponding author: A. Bishnu (abishnu@ed.ac.uk)

This work was supported in part by the Research Grant from Huawei Technologies (Sweden) AB.

ABSTRACT One of the approaches to support high data rates in beyond 5G cellular networks is the dense deployment of the small cell millimeter-wave (frequency range 2 (FR2)) (>24.5 GHz) base stations. However, this dense deployment of base stations leads to high cost, because it requires fiber backhaul connection with the core network. One prominent solution is the integrated access and backhaul (IAB) network proposed in 3GPP Release 16, where some portion of wireless spectrum is used for backhaul to serve base stations instead of fiber, and the remaining portion of the spectrum is used for user equipment for communication. The partition of the spectrum into access and backhaul degrades the spectral efficiency of the IAB network. Thus, in this paper, we propose a full-duplex (FD) enabled IAB network with large-scale array systems to enhance the spectral efficiency of the IAB network. In the FD IAB network, the IAB node is FD which transmits and receives at the same frequency/time resources. We consider a multi-cell multi-user IAB network with all the interferences due to FD transmission and evaluate the performance in terms of bit-error-rate and spectral efficiency. Moreover, an algorithm for choosing different users is proposed which is based on the cross-correlation of RF precoder weights. Further, identification of the optimal beam's index is also proposed which is based on the index of synchronization signal block and half-frame bit of physical broadcast channel payload of 5G NR. Finally, successive interference cancellation is proposed for self-interference mitigation in the digital domain.

INDEX TERMS Full-duplex, FR2, IAB network, RF precoder, 5G NR.

I. INTRODUCTION

5G and beyond technologies have ability to meet the demand of huge data rate in various wireless services through (i) mmWave spectrum (>24.5 GHz) known as frequency range 2 (FR2) which provides enormous bandwidth [1], and (ii) in-band full-duplex or full-duplex (FD), where an access point can simultaneously transmit and receive at the same time and frequency to provide better spectral efficiency [2]. However, the propagation characteristics of FR2 band limit the coverage area of mmWave communication which are completely different than that of FR1 (<7.125 GHz) band. Signals at FR2 band experience high path loss, severe atmospheric absorption, penetration loss, high attenuation due to rain, and large shadowing effect as compared to FR1 band. These artefacts become more severe as operating frequency increases [3], [4]. These huge losses at FR2 band can be mitigated by the state of art signal processing methods, such as highly directional narrow beamforming using large-scale array systems. A large-scale array system simultaneously exploits the enormous bandwidth of mmWave spectrum and high directional gain to support high speed and bandwidth-hungry wireless services [1].

It is also expected that advent of internet of things (IoT) leads to exponentially rise of the wireless devices. The cell size need to be smaller for serving these huge number of devices or users and hence leads to dense deployment of base stations or access points. These dense deployed base stations communicate with each other using fiber which tends to increase the cost of deployment causing expensive services to users. One prominent solution to reduce the cost of deployment of fiber is to use integrated access and backhaul (IAB) network that could make dense deployment economically feasible [5], [6]. In IAB network, IAB

The associate editor coordinating the review of this manuscript and approving it for publication was Ahmed Mohamed Ahmed Almradi.

donor (IABD) communicates with the core network using fiber and provides backhaul link to IAB node (IABN), whereas IABN communicates with IABD through backhaul link and with user equipment (UE) through access link. There is another architecture which includes multi-hopping in which the parent node (IABD) is connected to IABN through backhaul link and further the IABN is connected to child node (another IABN) through backhaul link [7]. In this way, some portion of the spectrum is used for backhaul and remaining is used for access link [8]. However, the partition of the spectrum into backhaul and access link deteriorates spectral efficiency of the IAB network. To enhance the spectral efficiency of IAB network, IABN can be enabled with FD, where IABN can simultaneously communicate with IABD and UE through backhaul and access link respectively at the same time and frequency.

In this paper, we evaluate the performance of multi-cell multi-user IAB network with FD enabled IABN for FR2 band specifically 28 GHz band in terms of bit-error-rate (BER) and spectral efficiency. We also evaluate the BER and spectral efficiency in the presence of intra-cell interference. In terms of self-interference (SI) cancellation, it is assumed that antenna-domain and analog-domain cancellation are already applied and only digital-domain SI cancellation is performed in this paper. Successive interference cancellation (SIC) is proposed to mitigate SI cancellation in digital-domain, where first the SI channel is estimated using physical data shared channel-demodulation reference signal (PDSCH-DMRS), and received signal. Then, the SI signal is decoded and subtracted from the received signal to obtain desired signal.

Further, only radio-frequency (RF) precoder and combiner are used for beamforming and also proposed the identification process of the optimal RF precoder vector index or beam index by UE using some operations of beam management and synchronization signal (SS) block of 5G NR. The beam index identification is based on the index of SS block (ssbIndex) and half frame bit of physical broadcast channel (PBCH) payload of 5G NR. This SS block is transmitted in a burst either in the first or second half of a radio frame which limits the total number of beams. The transmission of SS burst in a whole radio frame is proposed which increases the total number of beams and leads to better beam alignment (in terms of high received signal strength) between base station and UE. In addition, selection of users based on RF precoder weights is also proposed for mitigation of intra-cell interference. The proposed method for user selection is based on cross-correlation of RF precoder weights and chose only those users whose cross-correlation coefficient is less than some threshold.

The main contributions are summarized as:

- Evaluated the performance of fully loaded multi-cell, multi-user IAB network in terms of BER and spectral efficiency in the presence of additive white Gaussian noise (AWGN) and intra-cell interference.
- Implemented the identification procedure of index of the optimal RF precoder vector or beam by UE using beam management and SS block of 5G NR.
- Proposed algorithm for selection of users based on cross-correlation of RF precoder weights for mitigation of intra-cell interference.
- Proposed SIC for digital-domain SI cancellation.

Rest of the paper is organized as follows. Section II overviews the FD and IAB network, followed by system model of backhaul and access link in Section III. Section IV describes channel model for both SI and non-SI channel for FR2 band. After introducing the FR2 channel model, we provide detailed description of beam management and user selection in section V, where four methods of beam management and RF precoder weights based user selection as given in Algorithm 1 are discussed In Section VI, identification of beam index which is based on half frame bit of PBCH payload and ssbIndex of SS block of 5G broadcast channel is discussed. Section VII provides insight of details of SIC for digital-domain SI cancellation, followed by simulation results and discussion in Section VIII, and finally conclusions are drawn in Section IX.

II. FULL-DUPLEX COMMUNICATION AND IAB NETWORKS

In this section, we briefly discuss the FD communication and IAB networks.

A. FULL-DUPLEX COMMUNICATION

Recently, FD communication, where a transceiver can communicate with both uplink and downlink terminal using the same temporal and frequency resources, was introduced in [9]. FD is a key technology that could possibly double the spectral efficiency of a wireless system [10] and hence considered as promising technology for 5G beyond networks. Conventional communication is either half-duplex or out-of-band FD including time domain duplex and frequency domain duplex. In FD communication, a terminal can communicate with both uplink and downlink user, or terminal using same frequency band and time slot. The main challenge for FD communication is the SI caused by the transmitter on the receiver of the same transceiver. Typically the SI cancellation is done by antenna-domain SI followed by analog-domain SI cancellation and then finally by digital-domain SI cancellation as discussed below.

1) ANTENNA-DOMAIN SELF-INTERFERENCE CANCELLATION

In antenna cancellation technique, two transmit antennas are placed in such a way that their signal is received destructively at the receive antenna in the same transceiver. The distance offset between two transmit antennas from receive antenna must be half wavelength to achieve antenna SI cancellation. However, there is a fundamental limitation of antenna SI cancellation dependent on the bandwidth of the transmitted signal [11]. In antenna SI cancellation technique, only the

centre frequency signal is inverted in phase, and gets fully cancelled at the receive antenna. Due to the increase in bandwidth, a signal drifts from the centre frequency which leads to change in the phase offset of two versions from the transmit antenna. This change in frequency offset leads to imperfect inversion and does not cancel signal completely [11]. There is another way of SI cancellation by using different polarization of transmitted and received signal which leads to 20-30 dB SI cancellation.

2) ANALOG-DOMAIN SELF-INTERFERENCE CANCELLATION

The analog-domain SI cancellation method is used to mitigate the SI in analog chain before analog to digital converter (ADC). In analog-domain SI cancellation, the transmitted signal is split into two parts using either from power splitter or from Balun. One part is fed to antenna for transmission through the air and another part is fed to receiver of the same device using some analog devices such as phase shifter and attenuator, and finally subtracted from the received signal using power combiner. However, the phase shifter can be replaced by delay line. The analog-domain SI cancellation can be designed as channel-unaware or channel-aware techniques [12]. In the channel-unaware method, length of delay and gain of attenuator is fixed initially during calibration. The channel-unaware mechanism is suitable for narrow band system or direct path between transmitter and receiver [13]. In the channel-aware method, gain of the attenuator can be changed and it is based on received signal. The channel-aware method is suitable for both narrow and wideband system, or direct and reflected path between the transmitter and the receiver. The direct path cancellation is achieved in a similar way as in channel-unaware method, however the cancellation of reflected path is much more challenging [12]. For wideband system which occurs in FR2 band, the SI cancellation in RF-domain is not promising and leads to high losses because of more number of taps [14]. One promising solution is to cancel SI in optical-domain which shows better performance as compared to RF-domain for wideband system [14].

3) DIGITAL-DOMAIN SELF-INTERFERENCE CANCELLATION

Objective of the digital-domain SI cancellation is to remove remaining interference (which is still high as compared to desired signal) after analog-to-digital conversion (ADC) by using sophisticated digital signal processing. For wideband signal, multipath cancellation in analog-domain is difficult to design. Hence, tapping signal in the digital-domain and performing adaptive filtering is much easier to implement and faster [15]. However, the cancellation of residual SI in digital-domain is limited by ADC's dynamic range. Hence, the received SI signal before ADC should be in the dynamic range of the ADC so that after cancellation from digital domain, the residual SI reaches the noise floor. In the digital-domain SI cancellation, first the channel is estimated with the help of received and transmitted preamble or pilot using adaptive filtering. With the help of estimated channel coefficients and known transmitted preamble or pilots, noisy version of received signal is generated which is to be subtracted from the actual received signal.

B. INTEGRATED ACCESS AND BACKHAUL

LTE relaying for IAB is studied by 3GPP earlier in the scope of LTE Rel-10 [16]. However, due to expensiveness of existing LTE spectrum for backhauling, the deployment of LTE relaying is very limited and restricted. Further, 4G time frame had very limited scope for small cell deployments. Later, IAB is being standardized by 3GPP in rel-16 for 5G NR [16]. 5G NR has capability to provide more commercially successful deployment of IAB than LTE relaying because of mmWave communication which creates huge base station deployments, leading to the need of backhauling. Further, mmWave spectrum with huge bandwidth provides more economically feasible opportunity of backhauling. In addition, 5G NR has the capability of reducing cross-link interference between access and backhaul links by creating multi-beam signal using large-scale array system [5].

In an IAB network, an IABN can communicate with both UE and IABD through access and backhaul links, respectively as shown in Fig. 1, where an IABD can communicate with IABN and core network through backhaul link and optical fiber, respectively. It is also recognized by 3GPP that IAB is a practical and economical means of enabling 5G dense network [17]. It is expected that IABNs either communicate in stand alone (SA) mode or non-stand alone (NSA) mode. In SA mode, the node is connected to 5G network, while in NSA mode, it is connected to 4G evolved packet core [18]. There are two topologies under consideration (i) spanning tree where, one node is connected to each IABN, and (ii) directed acyclic graph where, various up-stream nodes are connected to IABNs. In both topologies, the IABN either serves as UE or as a parent or a child node connected to

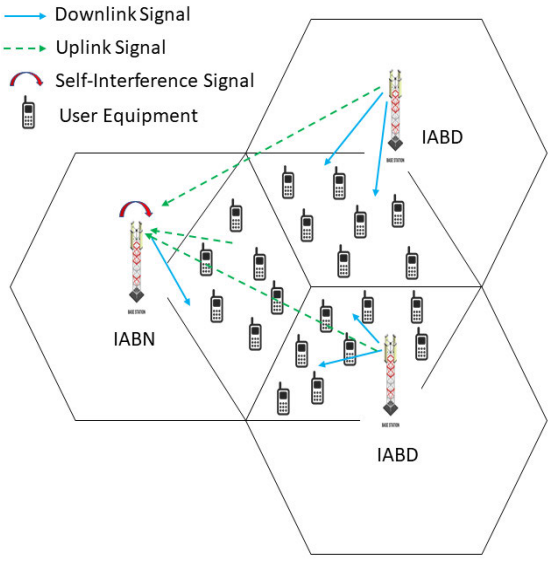

FIGURE 1. Architecture of IAB network with multi-cell multi-user scenario with FD at IABN.

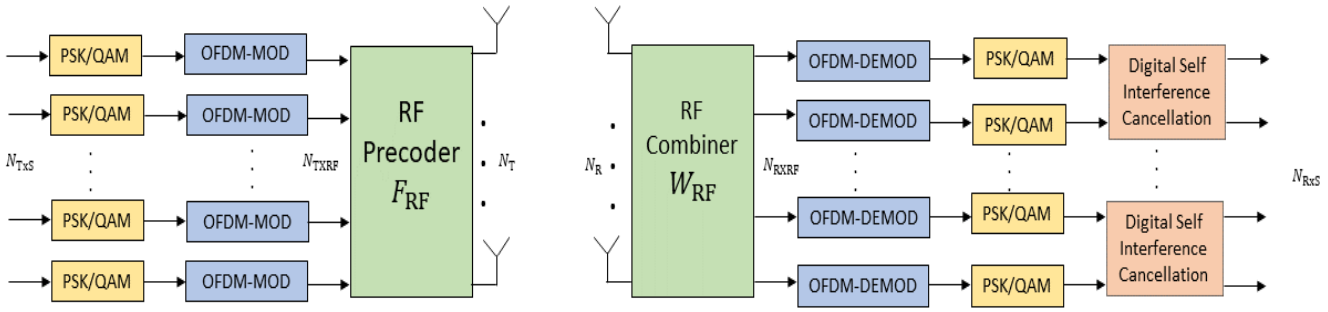

FIGURE 2. Large-scale array system with OFDM transceiver with RF/analog precoding for IABN.

other nodes [18]. Each IABN have two radio functions named as mobile termination (MT) and distributed unit (DU). MTs are used to provide wireless backhaul to IABD, while DUs are used to provide access to UEs [5].

Since, access and backhaul link communicate on traditional half-duplex radios, it leads to deterioration in the spectral efficiency and also introduce unwanted latency in the network. One prominent solution which has capability to overcome this issue is FD. We can employ FD at IABN as shown in Fig. 1, where IABN simultaneously communicate with two IABD through backhaul link, and downlink (DL) and uplink (UL) UEs through access link at the same time and frequency as given in [19]. Further, the IABD communicate with IABN and DL UEs through backhaul and access link simultaneously. The SI can be mitigated by using suitable analog and digital-domain algorithm at IABN as discussed in the previous subsection.

III. SYSTEM MODEL

Consider the N-FFT OFDM based large-scale array system model as shown in Fig. 2 for IABN with only analog/RF precoder, where a transmitter has N_{T} and N_{TXRF} transmit antenna and RF chain respectively, and N_{R} and N_{RXRF} receive antenna and RF chain respectively. The transmitter and receiver communicate via N_{TXS} and N_{RXS} independent data symbols respectively, such that $N_{\mathrm{TXS}} = N_{\mathrm{TXRF}} \ll N_{\mathrm{T}}$ and $N_{\mathrm{RXS}} = N_{\mathrm{RXRF}} \ll N_{\mathrm{R}}$.

At the transmitter, the N_{TXS} modulated data symbols (either QPSK or QAM) $s[k]$ at k^{th} subcarrier are converted into time-domain by using N-point IFFT followed by addition of cyclic prefix. The time-domain data symbols are fed to antennas through RF precoder matrix F_{RF} of dimension $N_{\mathrm{T}} \times N_{\mathrm{TXRF}}$. The F_{RF} is a block diagonal matrix represented as $\mathrm{Bdiag}[f_{\mathrm{RF},1}, \ldots, f_{\mathrm{RF},N_{\mathrm{sub}}}]$, and each f_{RF} have dimension $N_{\mathrm{T}}/N_{\mathrm{sub}} \times N^{t}_{\mathrm{RF}}$ (where N_{sub} (fixed) is the number of subarray, and N^{t}_{RF} (variable) is the number of RF chain connected to that $\mathrm{f_{RF}}$). The RF precoding matrix is used for transmitting the signal in a particular direction through antennas. The discrete time-domain transmitted complex symbol at n^{th} sample is given as:

$$x[n] = F_{\mathrm{RF}}[k]s'[n] \tag{1}$$

where $s'[n]$ is the discrete time-domain signal after OFDM modulation at n^{th} sample, and $|[f_{\mathrm{RF}}]_{m,m'}|^2 = 1$. The discrete frequency domain received complex symbol at k^{th} subcarrier is given as:

$$y[k] = W^{H}_{\mathrm{RF}} H[k] F_{\mathrm{RF}} s[k] + W^{H}_{\mathrm{RF}} n[k] \tag{2}$$

where W_{RF} is the RF combining matrix of dimension $N_{\mathrm{R}} \times N_{\mathrm{RXRF}}$, and it is also a block diagonal matrix represented as $\mathrm{Bdiag}[w_{\mathrm{RF},1}, \ldots, w_{\mathrm{RF},N_{\mathrm{sub}}}]$ and each w_{RF} have dimension $N_{\mathrm{R}}/N_{\mathrm{sub}} \times N^{r}_{\mathrm{RF}}$ (where N^{r}_{RF} (variable) is the number of RF chain connected to that $\mathrm{w_{RF}}$), $H[k]$ is the frequency domain channel matrix at k^{th} subcarrier of dimension $N_{\mathrm{R}} \times N_{\mathrm{T}}$, $n[k]$ is the additive white Gaussian noise (AWGN) vector.

The IABDs have 8 subarrays with equal antenna elements and 12 RF chain in total, where 4 subarrays have only one RF chain each and remaining 4 subarrays have two RF chain each. The two subarrays with one RF chain each communicate with two different IABN through backhaul link, while the rest of the RF chain are used for DL users. Similarly, IABN has 4 subarrays with two RF chain each in both transmit and receive section. The transmit section subarrays are used for DL users of IABN while in the receive section, one subarray with two RF chain communicate with two different IABD through backhaul link, and the remaining six RF chains are used for UL users of IABN. Both DL and UL users have one subarray with single RF chain. In the next few subsections, we discuss system model for different backhaul and access links.

A. IABD TO IABN BACKHAUL LINK

One of the subarray with single RF chain of both IABD communicate with one of the subarray with two RF chain of IABN. The discrete frequency-domain received complex symbol at k^{th} subcarrier at subarray 1 of IABN from subarray 1 of IABDs is given by (3), as shown at the bottom of the next page. The first two term of right hand side (RHS) of (3) is the desired signal from two IABD respectively, the third and fourth term of RHS of (3) are the strong and

weak SI signal respectively,[1] the fifth term of RHS of (3) is the intra-cell interference created by UL users and the last term of RHS of (3) represents AWGN. In (3), $w^{\mathrm{N}}_{\mathrm{RF},1}$ represents RF combiner for subarray 1 of IABN, $H^{\mathrm{ND1}}_{1,1}[k]$ and $H^{\mathrm{ND2}}_{1,1}[k]$ represent channel between subarray 1 of IABN and subarray of IABD 1, and that of IABD 2 respectively at k^{th} subcarrier. $f^{\mathrm{D1}}_{\mathrm{RF},1}$ and $f^{\mathrm{D2}}_{\mathrm{RF},1}$ represent RF precoder of subarray 1 of IABD 1 and IABD 2 respectively, $s^{\mathrm{ND1}}_{1}[k]$ and $s^{\mathrm{ND2}}_{1}[k]$ represent transmitted discrete frequency-domain signal to IABN from subarray 1 of IABD 1 and IABD 2 respectively at k^{th} subcarrier. $H^{\mathrm{SI}}_{1,i}[k]$ represents the SI channel from subarray i to subarray 1 of IABN at k^{th} subcarrier, $f^{\mathrm{N}}_{\mathrm{RF},1}$ represents RF precoder of subarray 1 of IABN to DL users, $s^{\mathrm{DLN}}_{1}[k]$ represents transmitted discrete frequency-domain signal from subarray 1 of IABN to DL users at k^{th} subcarrier. $f^{\mathrm{N}}_{\mathrm{RF},i}$ and $F^{\mathrm{NUL}}_{\mathrm{RF},j}$ represent RF precoder of i^{th} subarray of IABN for DL users and RF precoder of j^{th} UL user to IABN respectively, $s^{\mathrm{DLN}}_{i}[k]$ and $s^{\mathrm{NUL}}_{j}[k]$ represent transmitted discrete frequency-domain signal from i^{th} subarray of IABN to DL users and j^{th} UL user to IABN respectively at k^{th} subcarrier. $H^{\mathrm{NUL}}_{1,j}[k]$ represents channel between j^{th} UL user and subarray 1 of IABN at k^{th} subcarrier, $N^{\mathrm{IABN}}_{\mathrm{sub}}$ and NoUL denote number of subarray at IABN and number of UL users of IABN respectively, and κ represents cross polarization power ratio.

Since, the strong SI signal creates very high interference to the desired signal, it is not possible to decode the desired signal in the presence of such high SI. Hence, first the SI signal is estimated and then successive interference cancellation (SIC) is performed in digital-domain to remove SI and then finally decode the desired signal. The working of SIC in digital-domain SI cancellation will be discussed in later section.

B. IABD 1 TO DL USERS ACCESS LINK

The discrete frequency-domain received complex symbol at k^{th} subcarrier at i^{th} DL user from j^{th} subarray of IABD 1 with two RF chain is given as:

$$\begin{aligned} y^{\mathrm{DLD1}}_{i,2}[k] &= (W^{\mathrm{DLD1}}_{\mathrm{RF},i})^{H} H^{\mathrm{DLD1}}_{i,j}[k] f^{\mathrm{D1}}_{\mathrm{RF},j}(:,c) s^{\mathrm{DLD1}}_{j}(c,:)[k] \\ &\quad + (W^{\mathrm{DLD1}}_{\mathrm{RF},i})^{H} H^{\mathrm{DLD1}}_{i,j}[k] f^{\mathrm{D1}}_{\mathrm{RF},j}(:,d) s^{\mathrm{DLD1}}_{j}(d,:)[k] \\ &\quad + \sum_{a=1,a\neq j}^{N^{\mathrm{IABD}}_{\mathrm{sub}}} (W^{\mathrm{DLD1}}_{\mathrm{RF},i})^{H} H^{\mathrm{DLD1}}_{i,a}[k] f^{\mathrm{D1}}_{\mathrm{RF},a} s^{\mathrm{DLD1}}_{a}[k] \\ &\quad + (W^{\mathrm{DLD1}}_{\mathrm{RF},i})^{H} n^{\mathrm{DLD1}}[k] \end{aligned} \tag{4}$$

where first term of RHS of (4) represents the desired signal, second term of RHS of (4) represents interference from the different RF chain of same subarray, and third and last term of RHS of (4) denote interference from rest of the subarray of IABD 1 and AWGN respectively. $i \in [1,8], j \in [3,8], c \in [1,2], d \in [1,2]$, and $c \neq d$. $W^{\mathrm{DLD1}}_{\mathrm{RF},i}$ represents RF combiner of i^{th} DL user of IABD 1, $H^{\mathrm{DLD1}}_{i,j}[k]$ denote the channel between j^{th} subarray of IABD 1 and i^{th} DL user of IABD 1, s^{DLD1}_{j} denote the transmitted signal from j^{th} subarray to DL users of IABD 1 and $N^{\mathrm{IABD}}_{\mathrm{sub}}$ denotes number of subarray at IABD. $A(a,:)$ represents a^{th} row vector of A and $A(:,b)$ represents b^{th} column vector of A. The value of (i,j,c) for the desired signal are: (1,3,1), (2,3,2), (3,4,1), (4,4,2), (5,5,1), (6,5,2), (7,6,1), and (8,6,2). Similarly, the discrete frequency-domain received complex symbol at k^{th} subcarrier at i^{th} DL user from j^{th} subarray of IABD 1 with one RF chain is given as:

$$\begin{aligned} y^{\mathrm{DLD1}}_{i,1}[k] &= (W^{\mathrm{DLD1}}_{\mathrm{RF},i})^{H} H^{\mathrm{DLD1}}_{i,j}[k] f^{\mathrm{D1}}_{\mathrm{RF},j} s^{\mathrm{DLD1}}_{j}[k] \\ &\quad + \sum_{a=1,a\neq j}^{N^{\mathrm{IABD}}_{\mathrm{sub}}} (W^{\mathrm{DLD1}}_{\mathrm{RF},i})^{H} H^{\mathrm{DLD1}}_{i,a}[k] f^{\mathrm{D1}}_{\mathrm{RF},a} s^{\mathrm{DLD1}}_{a}[k] \\ &\quad + (W^{\mathrm{DLD1}}_{\mathrm{RF},i})^{H} n^{\mathrm{DLD1}}[k] \end{aligned} \tag{5}$$

where $i \in [9,10], j \in [3,8]$. The value of (i,j) for the desired signal are: (9,7), and (10,8).

The discrete frequency-domain received complex symbol at k^{th} subcarrier at i^{th} DL user of IABD 2 is expressed in a similar way as given in (4) and (5).

C. IABN TO DL USERS ACCESS LINK

The discrete frequency-domain received complex symbol at k^{th} subcarrier at i^{th} DL user from j^{th} subarray of IABN with two RF chain is given as:

$$\begin{aligned} y^{\mathrm{DLN}}_{i,2}[k] &= (W^{\mathrm{DLN}}_{\mathrm{RF},i})^{H} H^{\mathrm{DLN}}_{i,j}[k] f^{\mathrm{N}}_{\mathrm{RF},j}(:,c) s^{\mathrm{DLN}}_{j}(c,:)[k] \\ &\quad + (W^{\mathrm{DLN}}_{\mathrm{RF},i})^{H} H^{\mathrm{DLN}}_{i,j}[k] f^{\mathrm{N}}_{\mathrm{RF},j}(:,d) s^{\mathrm{DLN}}_{j}(d,:)[k] \\ &\quad + \sum_{a=1,a\neq j}^{N^{\mathrm{IABN}}_{\mathrm{sub}}} (W^{\mathrm{DLN}}_{\mathrm{RF},i})^{H} H^{\mathrm{DLN}}_{i,a}[k] f^{\mathrm{N}}_{\mathrm{RF},a} s^{\mathrm{DLN}}_{a}[k] \\ &\quad + \sum_{a=1}^{\mathrm{NoUL}} (W^{\mathrm{DLN}}_{\mathrm{RF},i})^{H} H^{\mathrm{NUL}}_{i,a}[k] F^{\mathrm{NUL}}_{\mathrm{RF},a} s^{\mathrm{NUL}}_{a}[k] \\ &\quad + (W^{\mathrm{DLN}}_{\mathrm{RF},i})^{H} n^{\mathrm{DLN}}[k] \end{aligned} \tag{6}$$

where first term of RHS of (6) represents the desired signal, second term of RHS of (6) represents interference from

$$\begin{aligned} y^{\mathrm{ND}}_{1}[k] &= (w^{\mathrm{N}}_{\mathrm{RF},1})^{H} H^{\mathrm{ND1}}_{1,1}[k] f^{\mathrm{D1}}_{\mathrm{RF},1} s^{\mathrm{ND1}}_{1}[k] + (w^{\mathrm{N}}_{\mathrm{RF},1})^{H} H^{\mathrm{ND2}}_{1,1}[k] f^{\mathrm{D2}}_{\mathrm{RF},1} s^{\mathrm{ND2}}_{1}[k] + 1/\sqrt{\kappa} (w^{\mathrm{N}}_{\mathrm{RF},1})^{H} H^{\mathrm{SI}}_{1,1}[k] f^{\mathrm{N}}_{\mathrm{RF},1} s^{\mathrm{DLN}}_{1}[k] \\ &\quad + 1/\sqrt{\kappa} \sum_{i=2}^{N^{\mathrm{IABN}}_{\mathrm{sub}}} (w^{\mathrm{N}}_{\mathrm{RF},1})^{H} H^{\mathrm{SI}}_{1,i}[k] f^{\mathrm{N}}_{\mathrm{RF},i} s^{\mathrm{DLN}}_{i}[k] + \sum_{j=1}^{\mathrm{NoUL}} (w^{\mathrm{N}}_{\mathrm{RF},1})^{H} H^{\mathrm{NUL}}_{1,j}[k] F^{\mathrm{NUL}}_{\mathrm{RF},j} s^{\mathrm{NUL}}_{j}[k] + (w^{\mathrm{N}}_{\mathrm{RF},1})^{H} n^{\mathrm{N}}[k] \end{aligned} \tag{3}$$

[1] We assume transmit and receive antennas are connected in same subarray with orthogonal polarization. Hence, the strong SI signal is only created by same subarray and rest of the subarray creates weak SI signal. For example, the transmitted signal from subarray 1 only creates strong SI to the received signal at subarray 1, while the transmitted signal from rest of the subarray creates weak SI to the received signal at subarray 1.

the different RF chain of same subarray, third and fourth term of RHS of (6) denote interference from rest of the subarray of IABN and UL users respectively, and the last term represents AWGN. $i \in [1,8], j \in [1,4], c \in [1,2], d \in [1,2]$, and $c \neq d$. $W_{\mathrm{RF},i}^{\mathrm{DLN}}$ represents RF combiner of i^{th} DL user of IABN, $H_{i,j}^{\mathrm{DLN}}[k]$ denote the channel between j^{th} subarray of IABN and i^{th} DL user of IABN, and s_j^{DLN} denote the transmitted signal from j^{th} subarray to DL users of IABN. The value of (i, j, c) for the desired signal are: (1,1,1), (2,1,2), (3,2,1), (4,2,2), (5,3,1), (6,3,2), (7,4,1), and (8,4,2).

D. UL USERS TO IABN ACCESS LINK

The discrete frequency-domain received complex symbol at k^{th} subcarrier at i^{th} subarray of IABN from j^{th} UL user is given by (7), as shown at the bottom of the page, where first term of RHS of (7) represents the desired signal, the second and third term of RHS of (7) are the strong and weak SI signal respectively, fourth term of RHS of (7) denotes interference from rest of the UL users of IABN, fifth and sixth term of RHS of (7) represent IABD 1 and IABD 2 signal respectively, and last term AWGN. $i \in [2,4], j \in [1,6], c \in [1,2]$, $w_{\mathrm{RF},i}^{\mathrm{N}}$ and $f_{\mathrm{RF},i}^{\mathrm{N}}$ denote RF combiner and precoder of i^{th} subarray of IABN respectively. $H_{i,j}^{\mathrm{NUL}}[k]$ and $H_{i,j}^{\mathrm{SI}}[k]$ represent the channel between j^{th} UL user and i^{th} subarray of IABN, and SI channel between j^{th} subarray of IABN and i^{th} subarray of IABN respectively at k^{th} subcarrier. $F_{\mathrm{RF},j}^{\mathrm{NUL}}$ is the RF precoder of j^{th} UL user of IABN, and $s_j^{\mathrm{NUL}}[k]$ and $s_i^{\mathrm{DLN}}[k]$ denote transmitted discrete frequency-domain signal of j^{th} UL user and i^{th} subarray of IABN respectively at k^{th} subcarrier. The value of (i, j, c) for the desired signal are: (2,1,1), (2,2,2), (3,3,1), (3,4,2), (4,5,1), (4,6,2).

IV. CHANNEL MODEL

The time-domain channel matrix $\mathbf{H}(\tau)$ at delay τ consists of line of sight (LOS) and non-line of sight (NLOS) given as [20]:

$$\mathbf{H}_{rs}(\tau) = \sqrt{\frac{K}{(1+K)}} h_{rs}^{\mathrm{LOS}} + \sqrt{\frac{1}{(K+1)}} \sum_{n=1}^{L} \sum_{m_n=1}^{M_n} h_{rs,n,m_n}^{\mathrm{NLOS}}(\tau - \tau_n - \tau_{m_n}) \quad (8)$$

where r and s represent r^{th} receive and s^{th} transmit antenna respectively. L is the number of clusters, M_n is the number of rays in n^{th} cluster. τ_n is the delay of n^{th} cluster, τ_{m_n} is the delay of m_n^{th} ray in n^{th} cluster, and K is the Rician factor. The complex channel gain for LOS and NLOS are given in [19].

The complex channel gain for LOS is given as [20]:

$$h_{rs}^{\mathrm{LOS}} = \begin{bmatrix} F_{\theta,GCS,r}(\theta_{\mathrm{LOS}}^{A}, \phi_{\mathrm{LOS}}^{A}) \\ F_{\phi,GCS,r}(\theta_{\mathrm{LOS}}^{A}, \phi_{\mathrm{LOS}}^{A}) \end{bmatrix}^{T} \begin{bmatrix} F_{\theta,GCS,s}(\theta_{\mathrm{LOS}}^{D}, \phi_{\mathrm{LOS}}^{D}) \\ F_{\phi,GCS,s}(\theta_{\mathrm{LOS}}^{D}, \phi_{\mathrm{LOS}}^{D}) \end{bmatrix} \times \mathrm{e}^{\mathrm{j}\frac{2\pi}{\lambda}(\mathbf{e_r}(\theta_{\mathrm{LOS}}^{A}, \phi_{\mathrm{LOS}}^{A})^{T}\mathbf{d_r})} . \mathrm{e}^{\mathrm{j}\frac{2\pi}{\lambda}(\mathbf{e_r}(\theta_{\mathrm{LOS}}^{D}, \phi_{\mathrm{LOS}}^{D})^{T}\mathbf{d_s})} \quad (9)$$

Similarly, the complex channel gain for NLOS is given as [20]:

$$h_{rs,n,m_n}^{\mathrm{LOS}} = \begin{bmatrix} F_{\theta,GCS,r}(\theta_{n,m_n}^{A}, \phi_{n,m_n}^{A}) \\ F_{\phi,GCS,r}(\theta_{n,m_n}^{A}, \phi_{n,m_n}^{A}) \end{bmatrix}^{T} \begin{bmatrix} F_{\theta,GCS,s}(\theta_{n,m_n}^{D}, \phi_{n,m_n}^{D}) \\ F_{\phi,GCS,s}(\theta_{n,m_n}^{D}, \phi_{n,m_n}^{D}) \end{bmatrix} \times \mathrm{e}^{\mathrm{j}\frac{2\pi}{\lambda}(\mathbf{e_r}(\theta_{n,m_n}^{A}, \phi_{n,m_n}^{A})^{T}\mathbf{d_r})} . \mathrm{e}^{\mathrm{j}\frac{2\pi}{\lambda}(\mathbf{e_r}(\theta_{n,m_n}^{D}, \phi_{n,m_n}^{D})^{T}\mathbf{d_s})} \quad (10)$$

where $F_{\theta,GCS,r}$ and $F_{\phi,GCS,r}$ are the radiation field patterns in the direction of the spherical basis vectors, $\mathbf{e}_\theta$ and $\mathbf{e}_\phi$ respectively of receive antenna element r, while $F_{\theta,GCS,s}$ and $F_{\phi,GCS,s}$ are the radiation field patterns in the direction of the spherical basis vectors, $\mathbf{e}_\theta$ and $\mathbf{e}_\phi$ respectively of transmit antenna element s. $\mathbf{e_r}$ is the spherical unit vector. $\theta_{\mathrm{LOS}}^{A}$ and ϕ_{LOS}^{A} are the elevation and azimuth angle of arrival (AoA) for LOS respectively. $\theta_{\mathrm{LOS}}^{D}$ and ϕ_{LOS}^{D} are the elevation and azimuth angle of departure (AoD) for LOS respectively. Φ_{LOS} is a random phase for LOS. $\mathbf{d_r}$ and $\mathbf{d_s}$ are the position vectors of the receive antenna element r and transmit antenna element s, given in global coordinate system (GCS). λ is the wavelength of the carrier frequency. θ_{n,m_n}^{A} and ϕ_{n,m_n}^{A} are the elevation and azimuth angle of arrival for m_n^{th} ray in n^{th} cluster respectively. θ_{n,m_n}^{D} and ϕ_{n,m_n}^{D} are the elevation and azimuth angle of departure for m_n^{th} ray in n^{th} cluster respectively.

The LOS component of SI channel is given as [21]:

$$h_{rs}^{\mathrm{LOS(SI)}} = \begin{bmatrix} F_{\theta,GCS,r}(\theta_{\mathrm{LOS}}^{A}, \phi_{\mathrm{LOS}}^{A}) \\ F_{\phi,GCS,r}(\theta_{\mathrm{LOS}}^{A}, \phi_{\mathrm{LOS}}^{A}) \end{bmatrix}^{T} \times \begin{bmatrix} F_{\theta,GCS,s}(\theta_{\mathrm{LOS}}^{D}, \phi_{\mathrm{LOS}}^{D}) \\ F_{\phi,GCS,s}(\theta_{\mathrm{LOS}}^{D}, \phi_{\mathrm{LOS}}^{D}) \end{bmatrix} \times \frac{1}{d_{rs}} \mathrm{e}^{-\mathrm{j}2\pi\frac{d_{rs}}{\lambda}} \quad (11)$$

where d_{rs} is the distance between s^{th} transmit antenna and r^{th} receive antenna. The NLOS component of SI channel is same as given in [20].

In the next section, we discuss beam management and user selection.

$$y_j^{\mathrm{NUL}}[k] = (w_{\mathrm{RF},i}^{\mathrm{N}}(:,c))^{H} H_{i,j}^{\mathrm{NUL}}[k] F_{\mathrm{RF},j}^{\mathrm{NUL}} s_j^{\mathrm{NUL}}[k] + \frac{1}{\sqrt{\kappa}} (w_{\mathrm{RF},i}^{\mathrm{N}}(:,c))^{H} H_{i,i}^{\mathrm{SI}}[k] f_{\mathrm{RF},i}^{\mathrm{N}} s_i^{\mathrm{DLN}}[k] + \frac{1}{\sqrt{\kappa}} \sum_{a=1,a\neq i}^{N_{\mathrm{sub}}^{\mathrm{IABN}}} (w_{\mathrm{RF},i}^{\mathrm{N}}(:,c))^{H} H_{i,a}^{\mathrm{SI}}[k] \times f_{\mathrm{RF},a}^{\mathrm{N}} s_a^{\mathrm{DLN}}[k] + \sum_{b=1,b\neq j}^{\mathrm{NoUL}} (w_{\mathrm{RF},i}^{\mathrm{N}}(:,c))^{H} H_{i,b}^{\mathrm{NUL}}[k] F_{\mathrm{RF},b}^{\mathrm{NUL}} s_b^{\mathrm{NUL}}[k] + (w_{\mathrm{RF,i}}^{\mathrm{N}}(:,c))^{H} H_{i,1}^{\mathrm{ND1}}[k] f_{\mathrm{RF},1}^{\mathrm{D1}} s_1^{\mathrm{ND1}}[k] + (w_{\mathrm{RF},1}^{\mathrm{N}}(:,c))^{H} \times H_{i,1}^{\mathrm{ND2}}[k] f_{\mathrm{RF},1}^{\mathrm{D2}} s_1^{\mathrm{ND2}}[k] + (w_{\mathrm{RF},i}^{\mathrm{N}})^{H} n^{\mathrm{N}}[k] \quad (7)$$

V. BEAM MANAGEMENT AND USER SELECTION

In this section, RF precoder weights design based on beam management and user selection based on the weights of RF precoder is discussed.

A. RF PRECODER WEIGHTS

In mmWave communication, the propagation loss is so high that reliable communication is not possible with MIMO system. Hence, a large-scale array system is required to provide reliable communication link between base station and UE which creates beamforming using high dimensional phased array. These high directional link, however, need proper direction of transmit and receive beam during communication, which is accomplished through a set of operations known as beam management. The beam management consists of four operations for stationary environments as [22], [23]:

- Beam Sweeping: A set of beams are transmitted and received according to pre-specified interval and resolution to cover a spatial area. Beam sweeping can be achieved by SS burst transmitted in either first half or second half of a 10 ms frame of 5G NR.
- Beam Measurement: In this step, quality of the received signal is measured at base station or UE either in terms of signal-to-noise (SNR) or received signal strength. In this paper, we used received signal strength as metric for quality of received signal.
- Beam Determination: It refers to selection of the appropriate beam or group of beam at both base station and UE based on beam measurement procedure.
- Beam Reporting: To exchange information about index of beam which is to be determined in the above step. The index of beam can be determined by the index of SS block of 5G NR.

The above set of operations are executed periodically to maintain the proper alignment of transmitter's and receiver's beam over time.

There are some control tasks which includes initial access (IA) and beam tracking. IA is used for stationary or non-movable users, which enables the base station and UE to establish a reliable physical link. If the users are non-stationary, then the beam tracking helps to maintain the reliable link between base station and UE [24]. The beam tracking can be achieved by channel state information-reference signal of 5G NR. In current LTE system, omnidirectional signal are used for control mechanisms, and then beamforming or other directional transmission are used for data transmission after reliable physical link is established. However in mmWave communication, both control mechanism which includes IA and beam tracking are also performed through directional transmission due to high propagation loss. Both IA and beam tracking procedure in mmWave communication increase the overall time of communication and also the performance is more prone to beam alignment. Moreover, both beam management mechanisms depend on many factors such as base station density, antenna geometry, beamforming configuration, and users' environment [24].

In this paper, beam sweeping is done into two parts in each sector (both IABD and IABN cellular area are divided into three sectors with 120° each as shown in Fig. 1.) as follows: (i) Divide the transmit antenna array of BS into number of subarrays with equal number of antenna elements in each subarray and each subarray transmits the SS burst at different non-overlapping azimuth and elevation angle of departure (AoD). While, the UE selects one random value of azimuth and elevation angle of arrival (AoA) as shown in Fig. 3. Now, the UE selects a beam based on beam measurement and determination, and feedback the beam index to BS through beam reporting; (ii) The BS transmits training signal with the feedback azimuth and elevation AoD and the UE sweeps the beam and select the optimum azimuth and elevation AoA using the same beam measurement and determination as shown in Fig. 4.

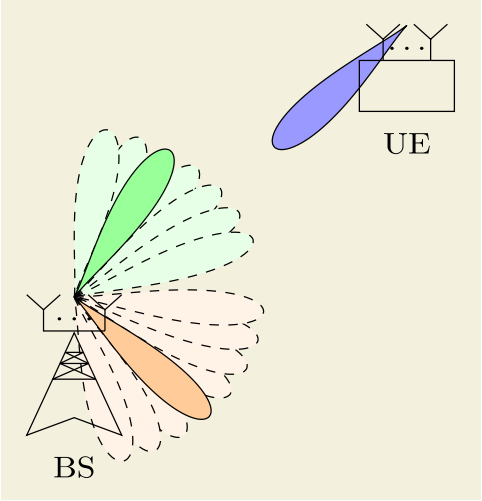

FIGURE 3. Beam sweeping by BS.

The beam management for IABD and IABN is discussed below.

1) IABD

IABD has eight subarrays and out of which two subarrays are used as backhaul link for communication with IABN. Since the position of IABD and IABN are fixed and hence azimuth and elevation AoD and AoA can be calculated using their position. For DL users of IABD with sector from 0° to 119°, the range of azimuth and elevation AoD of the remaining six subarrays are $\{\mathcal{S}_1^{\text{TXD}} = \phi_1^{\text{AoD}} \in [0, 19], \theta_1^{\text{AoD}} \in [1, 89]\}$, $\{\mathcal{S}_2^{\text{TXD}} = \phi_2^{\text{AoD}} \in [20, 39], \theta_2^{\text{AoD}} \in [1, 89]\}$, $\{\mathcal{S}_3^{\text{TXD}} = \phi_3^{\text{AoD}} \in [40, 59], \theta_3^{\text{AoD}} \in [1, 89]\}$, $\{\mathcal{S}_4^{\text{TXD}} = \phi_4^{\text{AoD}} \in [60, 79], \theta_4^{\text{AoD}} \in [1, 89]\}$, $\{\mathcal{S}_5^{\text{TXD}} = \phi_5^{\text{AoD}} \in [80, 99], \theta_5^{\text{AoD}} \in [1, 89]\}$, and $\{\mathcal{S}_6^{\text{TXD}} = \phi_6^{\text{AoD}} \in [100, 119], \theta_6^{\text{AoD}} \in [1, 89]\}$. The DL users can choose any one value for azimuth and elevation AoA from $\{\mathcal{S}^{\text{RXD}} = \phi^{\text{AoA}} \in [0, 359], \theta^{\text{AoA}} \in [91, 179]\}$ randomly.

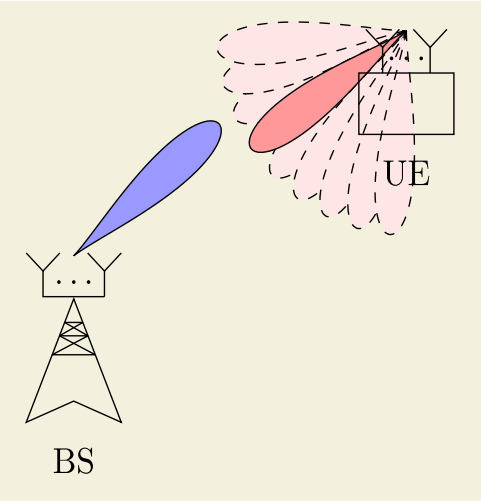

FIGURE 4. Beam sweeping by UE.

Let the received discrete time-domain signal for DL user is given by $y^{\mathrm{DLD}}[n]$ and the index of the optimum azimuth and elevation AoD are calculated as:

$$\{\hat{\phi}_{\mathrm{ID}}^{\mathrm{AoD}}, \hat{\theta}_{\mathrm{ID}}^{\mathrm{AoD}}\} = \max_{\{\mathcal{S}_1^{\mathrm{TXD}}, \mathcal{S}_2^{\mathrm{TXD}}, \mathcal{S}_3^{\mathrm{TXD}}, \mathcal{S}_4^{\mathrm{TXD}}, \mathcal{S}_5^{\mathrm{TXD}}, \mathcal{S}_6^{\mathrm{TXD}}\}} |y^{\mathrm{DLD}}[n]\{\phi^{\mathrm{AoA}}, \theta^{\mathrm{AoA}}\}|^2 \tag{12}$$

The calculated index of AoD is sent back to the base station through some feedback channel in beam reporting.

Now, the base station choose the optimum AoD based on index given by DL user and transmit the training signal with the chosen AoD. The DL user varies azimuth and elevation AoA with mean $\{\phi^{\mathrm{AoA}}, \theta^{\mathrm{AoA}}\}$ which is taken initially through beam sweeping to achieve $\{\hat{\theta}^{\mathrm{AoA}}, \hat{\phi}^{\mathrm{AoA}}\}$ as shown in Fig. 4. Finally, AoD and AoA values are achieved for which the reliable communication occurs.

2) IABN

Since the IABN has four subarray, hence the transmit antenna array is divided into four subarray with range of azimuth and elevation AoD are $\{\mathcal{S}_1^{\mathrm{TXN}} = \phi_1^{\mathrm{AoD}} \in [0, 29], \theta_1^{\mathrm{AoD}} \in [1, 89]\}$, $\{\mathcal{S}_2^{\mathrm{TXN}} = \phi_2^{\mathrm{AoD}} \in [30, 59], \theta_2^{\mathrm{AoD}} \in [1, 89]\}$, $\{\mathcal{S}_3^{\mathrm{TXN}} = \phi_3^{\mathrm{AoD}} \in [60, 89], \theta_3^{\mathrm{AoD}} \in [1, 89]\}$, and $\{\mathcal{S}_4^{\mathrm{TXN}} = \phi_4^{\mathrm{AoD}} \in [90, 119], \theta_4^{\mathrm{AoD}} \in [1, 89]\}$. While, rest of the procedure is same as for IABD with replacement of $y^{\mathrm{DLD}}[n]$ with DL user of IABN $y^{\mathrm{DLN}}[n]$.

In this way, the weights of RF precoder and combiner are calculated through beam management for IABD, IABN and DL users.

B. USER SELECTION

In this subsection, we proposed user selection based on the weights of RF precoder to mitigate intra-cell interference as given in Algorithm 1. The algorithm is based on cross-correlation of RF precoder columns and chooses those columns whose cross-correlation to other columns are less than some threshold (Th). 'length' in the algorithm represents length of the input vector. There is probability that some users form a cluster and hence causes interference which limits the performance of the network. In this case, some scheduling is to be performed to obtain satisfactory network performance.

Algorithm 1 User Selection

Input: F_{RF} (IABD and IABN)
Output: Ind (User Index)

```
L ← # of column of F_RF, l ← 2,Ind ← 1;
while l < L+1 do
    for w ← 1: length(Ind) do
        C ← abs(F_RF(:, Ind(w))^H F_RF(:, l));
        if C < Th then
            Ind ← [Ind l];
        else
            Ind ← Ind;
    if length(Ind)> 2 then
        if length(Ind) == 2*w then
            Ind ← Ind(1:w+1);
        else
            Ind ← Ind(1:w);
    l ← l + 1;
    if length(Ind) == # of users supported by BS then
        break;
```

To mitigate the ICI between users a method of users' selection is proposed in algorithm 1. Theoretically, the ICI should be zero to achieve optimal users' selection and this can be fulfilled if two RF beams are orthogonal to each other which leads cross-correlation (C) tends to zero. The beams consist of one main lobe and few side lobes with reduced power. The main lobe of two RF beams can be orthogonal but, the sidelobes may not. The power of side lobes tends to zero for infinite number of antenna elements and which is impractical. Hence, the value of threshold (Th) can be chosen according to the acceptable BER of different type of services.

VI. BEAM INDEX DETERMINATION

In this section, index of beam or column of RF precoder matrix determination at UE is discussed based on 5G NR standard. Each column of RF precoder matrix which is also known as beam represents the index which is to be identified by the UE in beam determination step and feedback the same index information to base station. The beam index identification can be done by using SS block of 5G NR.

The SS block also known as synchronization/PBCH block is the most important for synchronization of base station and UE. It consists of four consecutive OFDM symbols with 240 subcarriers each [25] as shown in Fig. 5. The primary synchronization signal (PSS) placed in first OFDM symbol and secondary synchronization signal (SSS) placed in third OFDM symbol are jointly used to identify the physical cell

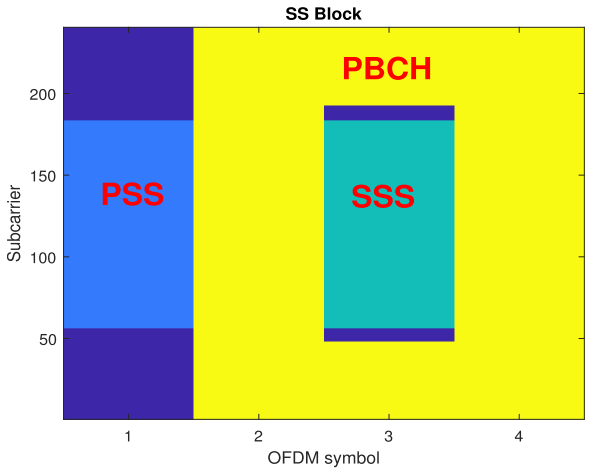

FIGURE 5. Synchronization signal block of 5G NR.

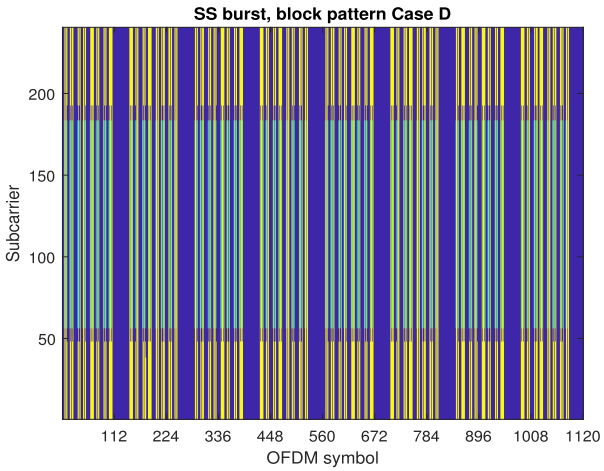

FIGURE 6. SS burst for whole 10 ms frame.

ID (PCI) of base station (gNodeB for 5G NR). Both PSS and SSS have same length of 127 subcarriers. There are three PSS sequence and 336 SSS sequence which creates 1008 PCI. The PBCH consists of PBCH payload and PBCH-DMRS placed in second, third and fourth OFDM symbol, and are QPSK modulated. The SS block is used for frame synchronization, carrier frequency offset estimation. The length of PBCH is 576 subcarriers, out of which 144 subcarriers are used for PBCH-DMRS. PBCH-DMRS is used for channel estimation by which PBCH payload is equalized and demodulated. PBCH payload carries broadcast channel (BCH) payload which includes CHOICE bit and master information block (MIB), system frame number and active reception of data or control channels [26]. MIB carries crucial information for decoding of system information block Type 1. The length of PBCH payload is 32 bits including BCH payload of length 24 bits (CHOICE bit is 1 bit and remaining 23 bit represents MIB), and 8 bits additional timing bits. The PBCH payload is appended by 24 bits cyclic redundancy check (CRC). SS block is transmitted in a burst known as SS burst and 64 SS blocks are transmitted in a SS burst for mmWave with 400 MHz bandwidth (Case D). These SS burst is transmitted in either first half or the second half of a 10 ms frame. Each SS block in a burst is transmitted with different beam which leads to 64 different beams in a frame. The transmission of a SS burst only in half of the frame leads to low resolution of beams which may causes beam alignment with degraded performance of received signal strength. To this end, transmission of SS burst in a whole frame is proposed which leads to 128 SS block in a frame as shown in Fig. 6, hence improve the received signal strength by transmitting more number of beams in a frame.

Two fields of PBCH payload named as ssbIndex and half frame bit are used for beam index. The length of SS block index and half frame bit are 6 and 1 bit respectively, which gives total 7 bits and 128 index for beam or column of RF precoder. The structure of PBCH payload is shown in Fig. 7, which includes 24 bit of PBCH payload, 4 bit (out of 10 bit) of

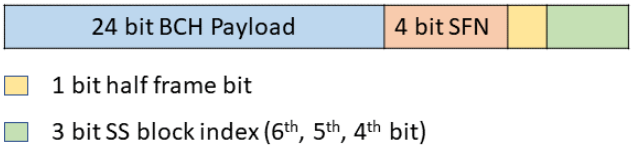

FIGURE 7. PBCH payload of 5G NR.

system frame number, 1 bit half frame bit, and 3 bit (out of 6 bit) of ssbIndex. The remaining 3 bit of ssbIndex are used to generate PBCH-DMRS symbol in conjunction with PCI. The half frame bit is '0' and '1' for first half and second of the frame respectively. The magnitude of the received signal at UE with different beam for each SS block for a frame is shown in Fig. 8. The steps for decoding the beam index at UE are as follows:

- Identify the starting time of the SS block for which the received signal strength is the highest with the help of PSS in time domain.

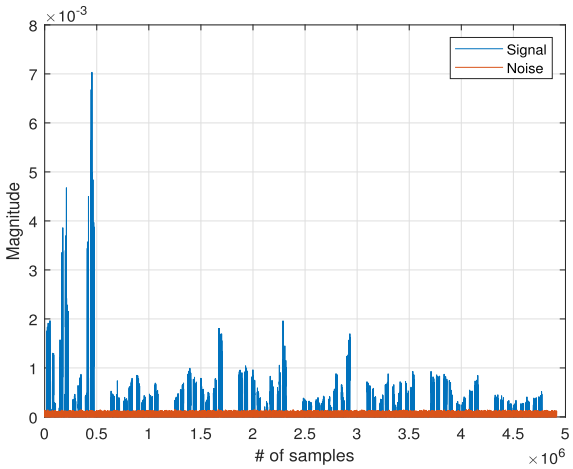

FIGURE 8. Magnitude of received signal for 128 different beam.

- Identify the sequence of SSS in frequency domain, and finally determine the PCI with the help of both PSS and SSS.
- Generate PBCH-DMRS symbols locally using PCI and all 8 combination of 3 bit of SS block index. There is only combination of ssbIndex for which CRC gives zero and that combination is the actual 3 bit of ssbIndex.
- The generated PBCH-DMRS is used for channel estimation and the estimated channel is used for equalization of PBCH payload symbols.
- The PBCH payload bits are demodulated and decoded, and retrieve the half frame bit and remaining 3 bit of ssbIndex.
- Finally beam index is calculated using retrieved half frame bit and 6 bit of ssbIndex which is feedback to base station.

VII. DIGITAL SELF-INTERFERENCE CANCELLATION

The IABN is FD enabled and hence SI cancellation is to be performed for reliable decoding of UL users through access link and IABD signal through backhaul link. It is assumed that both antenna and analog-domain SI cancellation is done and digital-domain SI cancellation is discussed in this section. The algorithm used in digital-domain SI cancellation is SIC. In SIC, first the SI channel is estimated followed by multiplication with the transmitted SI symbol then subtracted from the received signal which gives the desired signal. The PDSCH-DMRS is used as pilot for channel estimation. The frequency-domain received signal matrix at k_p pilot subcarrier at subarray 1 of IABN for IABD is given as:

$$\begin{aligned} Y_1^{\mathrm{ND}}[k_p] &= H_{\mathrm{eff1},1}^{\mathrm{ND1}}[k_p]S_1^{\mathrm{ND1}}[k_p] + H_{\mathrm{eff1},1}^{\mathrm{ND2}}[k_p]S_1^{\mathrm{ND2}}[k_p] \\ &\quad + H_{\mathrm{eff1},1}^{\mathrm{SI}}[k_p]S_1^{\mathrm{DLN}}[k_p] + \sum_{i=2}^{N_{\mathrm{sub}}^{\mathrm{IABN}}} H_{\mathrm{eff1},i}^{\mathrm{SI}}[k_p]S_i^{\mathrm{DLN}}[k_p] \\ &\quad + \sum_{j=1}^{\mathrm{NoUL}} H_{\mathrm{eff1},j}^{\mathrm{NUL}}[k_p]s_j^{\mathrm{NUL}}[k_p] + (w_{\mathrm{RF},1}^{\mathrm{N}})^H n^{\mathrm{N}}[k_p] \end{aligned} \quad (13)$$

where first two term of RHS of (13) represent the desired signal from IABD1 and IABD2 respectively, third and fourth term of RHS of (13) represent strong and weak SI, last two term of RHS of (13) represents UL user interference of IABN and AWGN respectively. $H_{\mathrm{eff1},1}^{\mathrm{ND1}}[k_p] = (w_{\mathrm{RF},1}^{\mathrm{N}})^H H_{1,1}^{\mathrm{ND1}}[k_p] f_{\mathrm{RF},1}^{\mathrm{D1}}$, $H_{\mathrm{eff1},1}^{\mathrm{ND2}}[k_p] = (w_{\mathrm{RF},1}^{\mathrm{N}})^H H_{1,1}^{\mathrm{ND2}}[k_p] f_{\mathrm{RF},1}^{\mathrm{D2}}$, $H_{\mathrm{eff1},i}^{\mathrm{SI}}[k_p] = (w_{\mathrm{RF},1}^{\mathrm{N}})^H H_{1,i}^{\mathrm{SI}}[k_p] f_{\mathrm{RF},i}^{\mathrm{N}}$, $H_{\mathrm{eff1},j}^{\mathrm{NUL}}[k_p] = (w_{\mathrm{RF},1}^{\mathrm{N}})^H H_{1,j}^{\mathrm{NUL}}[k] F_{\mathrm{RF},j}^{\mathrm{NUL}}$, $S_1^{\mathrm{ND1}}[k_p]$ and $S_1^{\mathrm{ND2}}[k_p]$ are the pilot signals of subarray 1 of IABD 1 and IABD 2 respectively, and $S_i^{\mathrm{DLN}}[k_p]$ and $s_j^{\mathrm{NUL}}[k_p]$ are the pilot signals of subarray i^{th} of IABN and j^{th} UL user of IABN respectively. The pilot position of $S_1^{\mathrm{ND1}}[k_p]$ and $S_1^{\mathrm{ND2}}[k_p]$ are orthogonal. Since $S_1^{\mathrm{DLN}}[k]$ is the strongest signal, hence first decode this strongest signal with the help of $S_1^{\mathrm{DLN}}[k_p]$ and $\hat{H}_{\mathrm{eff1},1}^{\mathrm{SI}}[k_p]$ ($\hat{H}_{\mathrm{eff1},1}^{\mathrm{SI}}[k_p]$ is the estimated of $H_{\mathrm{eff1},1}^{\mathrm{SI}}[k_p]$).

Initially $\hat{H}_{\mathrm{eff1},1}^{\mathrm{SI}}[k_p]$ can be calculated as:

$$\hat{H}_{\mathrm{eff1},1}^{\mathrm{SI}}[k_p] = Y_1^{\mathrm{ND}}[k_p]\Big((S_1^{\mathrm{DLN}}[k_p])^H S_1^{\mathrm{DLN}}[k_p]\Big)^{-1} \times (S_1^{\mathrm{DLN}}[k_p])^H \quad (14)$$

The channel coefficients at the remaining subcarriers are calculated by interpolation on the estimated channel coefficients at k_p pilot subcarrier. Finally, $\hat{S}_1^{\mathrm{DLN}}[k]$ can be calculated as:

$$\hat{S}_1^{\mathrm{DLN}}[k] = \Big((\hat{H}_{\mathrm{eff1},1}^{\mathrm{SI}}[k])^H \hat{H}_{\mathrm{eff1},1}^{\mathrm{SI}}[k]\Big)^{-1} Y_1^{\mathrm{ND}}[k] \quad (15)$$

Then the estimated frequency-domain received signal of subarray 1 of IABD 1 at subarray 1 of IABN $Y^{\mathrm{DR}}[k]$ can be evaluated as:

$$\hat{Y}_1^{\mathrm{ND1}}[k] = Y_1^{\mathrm{ND}}[k] - \hat{H}_{\mathrm{eff1},1}^{\mathrm{SI}}[k]\hat{S}_1^{\mathrm{DLN}}[k] \quad (16)$$

Then, $\hat{H}_{\mathrm{eff1},1}^{\mathrm{ND1}}[k_p]$ can be calculated as:

$$\hat{H}_{\mathrm{eff1},1}^{\mathrm{ND1}}[k_p] = \hat{Y}_1^{\mathrm{ND1}}[k_p]\Big((S_1^{\mathrm{ND1}}[k_p])^H S_1^{\mathrm{ND1}}[k_p]\Big)^{-1} \times (S_1^{\mathrm{ND1}}[k_p])^H \quad (17)$$

and finally decode $\hat{S}_1^{\mathrm{ND1}}[k]$ as:

$$\hat{S}_1^{\mathrm{ND1}}[k] = \Big((\hat{H}_{\mathrm{eff1},1}^{\mathrm{ND1}}[k])^H \hat{H}_{\mathrm{eff1},1}^{\mathrm{ND1}}[k]\Big)^{-1} \hat{Y}_1^{\mathrm{ND1}}[k] \quad (18)$$

In the same way, $\hat{S}_1^{\mathrm{ND2}}[k]$ can be decoded.

The UL users of IABN also experienced SI and hence SIC is also applied for UL users signal before decoding their desired signal at IABN. It is also to be noted that the pilot positions for the UL users of same subarray of IABN are orthogonal to each other. The same procedure as given in (14)-(18) is applied for each UL user to reliably decode their signal.

VIII. SIMULATION RESULTS AND DISCUSSION

In this section, we evaluate the performance of multi-cell multi-user large-scale array system FD enabled IAB network scenario in terms of BER and spectral efficiency. The simulation parameters are taken from 5G NR [27], where carrier frequency and bandwidth are chosen as 28 GHz and 400 MHz respectively. FFT size is 4096, number of data subcarrier is 3300, and number of PDSCH- DMRS is 1650 and 825 for IABN and IABD respectively. Number of antenna at IABD and IABN are 512 and 256 in each sector respectively. The IABD's antennas are divided into 8 subarray and each subarrays have equal number of non-overlap antenna elements. Out of eight subarrays, two subarrays with singe RF chain each are communicate with IABN through backhaul link, two subarrays with single RF chain each are used for serving two DL users through access link, and the remaining four subarrays with two RF chain each are used for serving eight DL users through access link. Similarly, the IABN's antennas are divided into 4 subarrays and each subarrays have equal number of non-overlap antenna elements for both transmitter

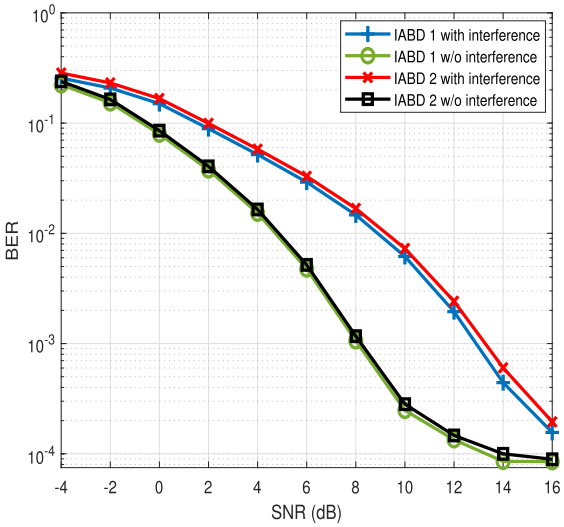

FIGURE 9. BER vs. SNR of QPSK modulation of IABDs to IABN.

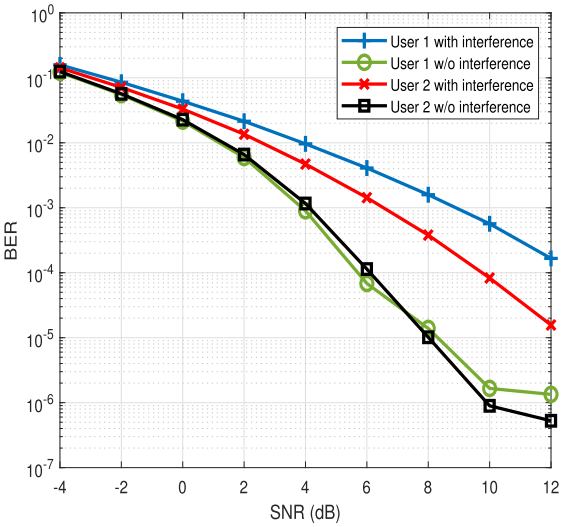

FIGURE 11. BER vs. SNR of QPSK modulation of UL users of IABN.

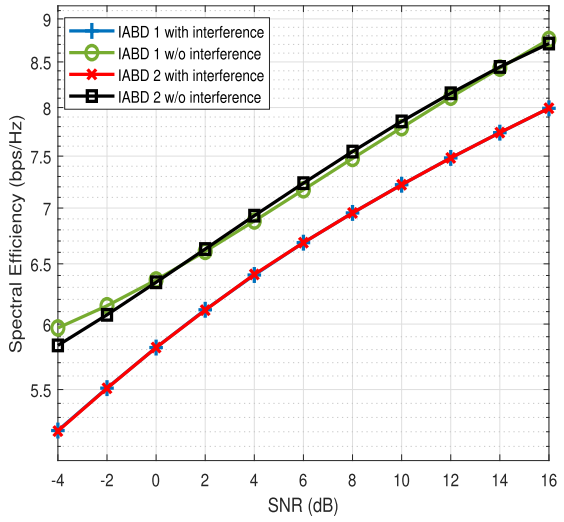

FIGURE 10. Spectral efficiency vs. SNR for IABDs.

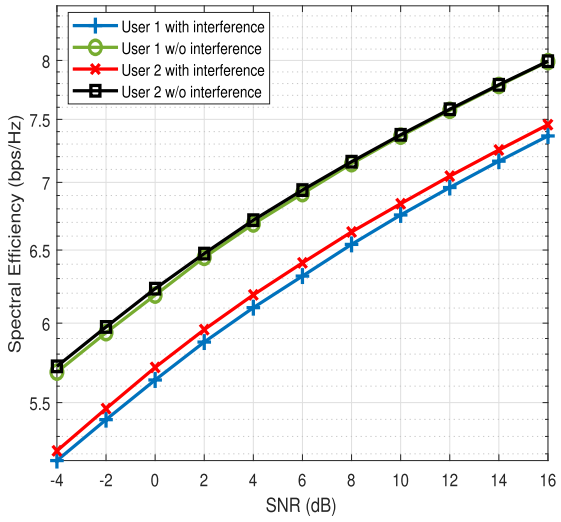

FIGURE 12. Spectral efficiency vs. SNR for UL users of IABN.

and receiver section. In the transmit section, all four subarrays with two RF chain each are used for 8 DL users through access link, while in receive section, three subarrays with two RF chain each are used for serving 6 UL users through access link whereas, one subarray with two RF chain communicates with two IABD through backhaul link. Each UE have 32 antenna elements with single RF chain. PDSCH-DMRS are distributed in the first two OFDM symbols and their positions are orthogonal for each subarrays of IABN and IABD). The transmit and receive antennas are orthogonally polarized. PDSCH data is low density parity check (LDPC) encoded with code rate 1/3. The channel is generated using ray-tracing channel simulator with height of IABD, IABN, and UE are 20m, 15m, and 1.5m respectively. The value of cross polarization power ratio is assumed to be 21 dB [28]. It is assumed that the antenna-domain and analog-domain SI cancellation are done at the IABN before converting the received signal into digital domain. Further, digital-domain SI cancellation is done by using successive interference cancellation as discussed in Section VII.

Fig. 9 shows the BER vs. SNR of QPSK modulated IABDs signal to subarray 1 of IABN with and without intra-cell interference in the presence of AWGN and SI signal. The interference to IABDs signal is caused by six UL users of IABN and the other IABD. The error floor of IABDs signal without interference is due to the presence of residual SI remaining after digital-domain SI cancellation. Fig. 10 shows the spectral efficiency of two IABDs with and without interference in the presence of AWGN and SI signal. Fig. 11 shows the BER vs. SNR of QPSK modulated UL users signal to subarray 2 of IABN with and without intra-cell interference in the presence of AWGN and SI signal. The interference to

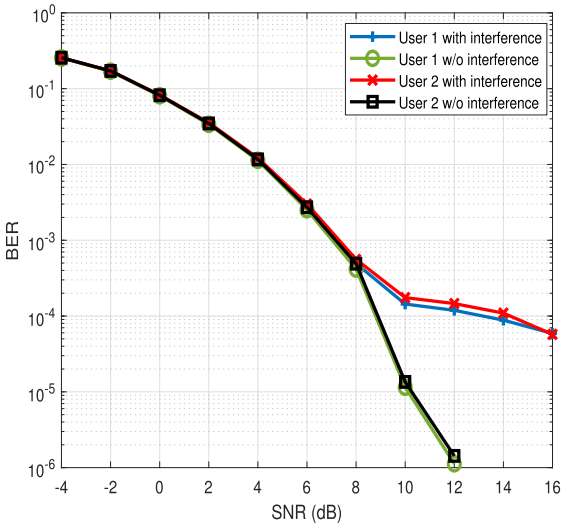

FIGURE 13. BER vs. SNR of QPSK modulation of DL users of IABD.

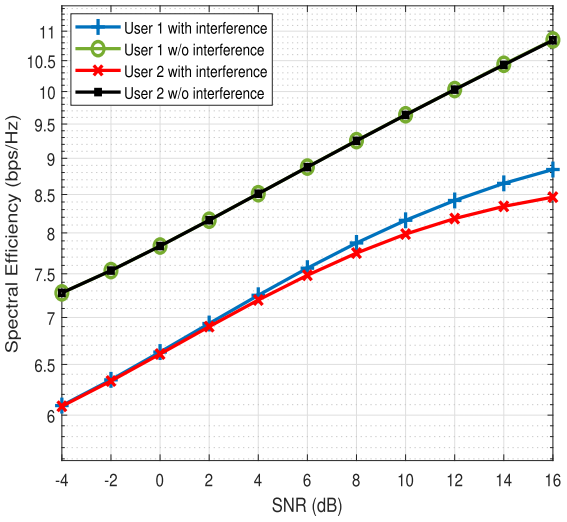

FIGURE 14. Spectral efficiency vs. SNR for DL users of IABD.

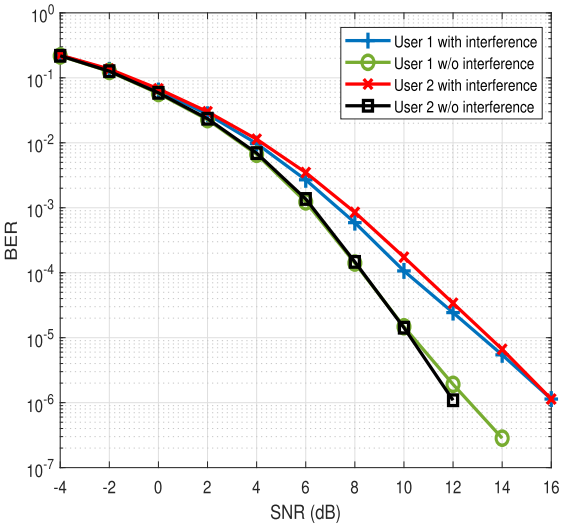

FIGURE 15. BER vs. SNR of QPSK modulation of DL users of IABN.

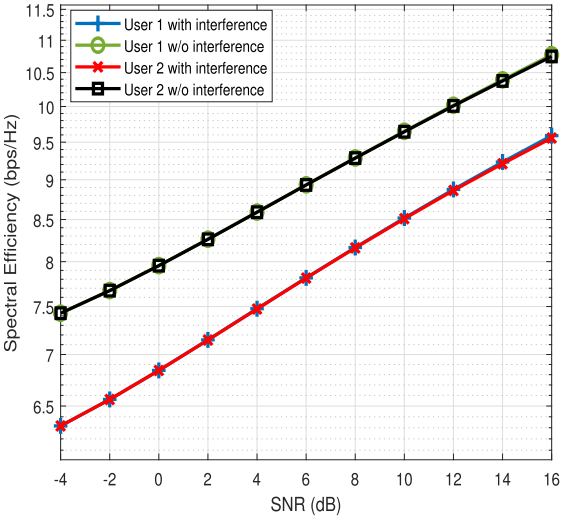

FIGURE 16. Spectral efficiency vs. SNR for DL users of IABN.

UL users signal is caused by the remaining four UL users of IABN and IABDs signal. The error floor of UL users signal without interference is again due to the presence of residual SI remaining after digital-domain SI cancellation. Fig. 12 shows the spectral efficiency of two UL users of subarray 2 of IABN with and without interference in the presence of AWGN and SI signal. It is concluded from the Figs. that residual SI limits the BER performance, however the amount of residual SI depends on the SI power to desired signal power ratio (SIDR) at receiver. If SIDR is high and within the dynamic range of an ADC, then the residual SI is nearly equal to noise level due to low channel estimation error.

Fig. 13 shows the BER vs. SNR of QPSK modulated DL users of subarray 3 of IABD 1 with and without intra-cell interference in the presence of AWGN. The interference is caused by remaining 8 DL users of IABD 1. The error floor in the interference is due to the presence of at least one interfering DL user in the vicinity of the desired DL user. Fig. 14 shows the spectral efficiency of two DL users of subarray 3 of IABD 1 with and without interference in the presence of AWGN. Fig. 15 shows the BER vs. SNR of QPSK modulated of DL users of subarray 1 of IABN with and without intra-cell interference in the presence of AWGN. The interference is caused by the remaining six DL users of IABN and six UL users of IABN. Fig. 16 shows the spectral efficiency of two DL users of subarray 1 of IABN with and without interference in the presence of AWGN. It is concluded from the Figs. that the interfering users degrade the BER performance of desired user if their position is in the vicinity of the desired user. So, in that case some scheduling has to performed for reliable communication.

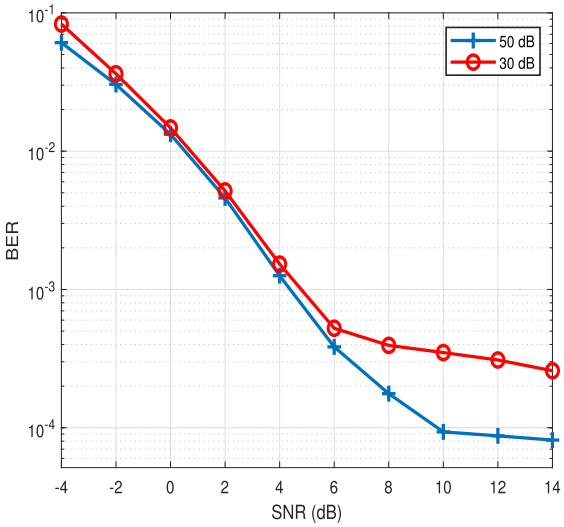

FIGURE 17. BER vs. SNR of QPSK modulation of DL users of IABN.

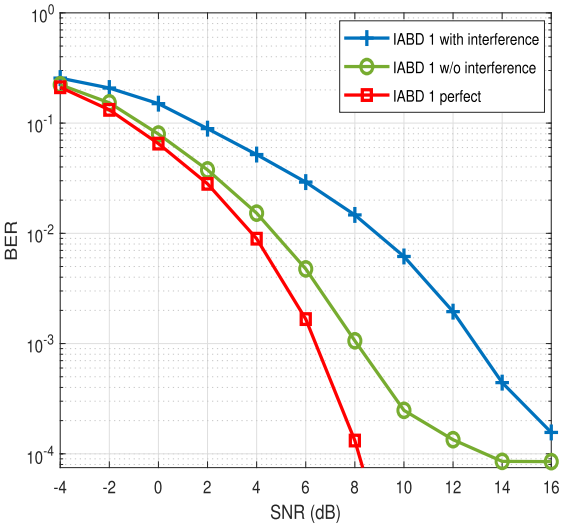

FIGURE 19. BER vs. SNR of QPSK modulation of DL users of IABN.

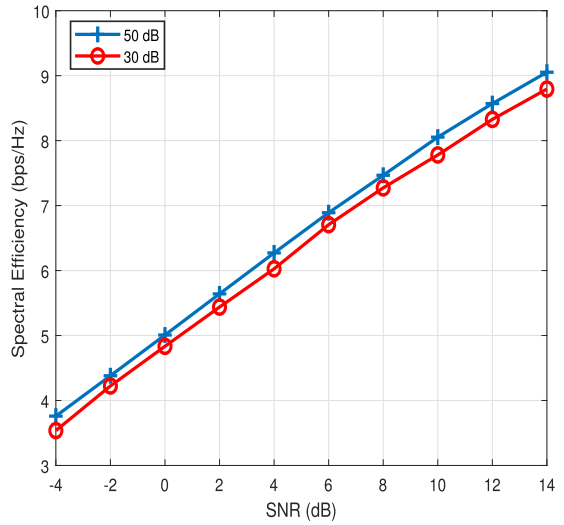

FIGURE 18. BER vs. SNR of QPSK modulation of DL users of IABN.

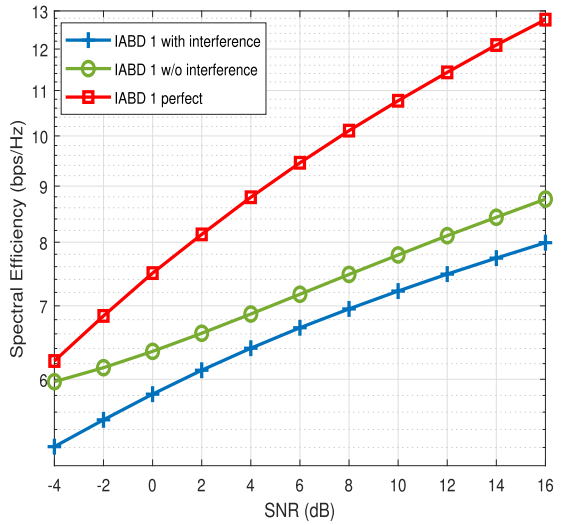

FIGURE 20. BER vs. SNR of QPSK modulation of DL users of IABN.

In addition, we provide an interesting insight of amount of analog-domain cancellation on BER and spectral efficiency performance which is also evident from simulations. The power of self-interference (SI) received signal is too large to saturate the ADC, and hence analog-domain cancellation of SI is required. However, if the ratio of SI signal after analog-domain cancellation to the desired signal is high (due to the small amount of SI cancellation in analog-domain), it leads to better channel estimation which further causes better SI cancellation in digital-domain and finally improves the BER and spectral efficiency performance. On the contrary, if the ratio of SI signal after analog-domain cancellation to the desired signal is low (due to the large amount of SI cancellation in analog-domain), it leads to poor channel estimation which further causes poor SI cancellation in digital-domain and finally deteriorates the BER, and spectral efficiency performance as shown in Fig. 17 and 18. Fig. 17 shows the BER vs. SNR for QPSK modulated of IABD 1 user to IABN in the presence of residual SI for different values of the ratio of SI signal after analog-domain cancellation to the desired signal. It is evident from the Fig. 17 that the BER performance is better for high value of ratio of SI signal after analog-domain cancellation to the desired signal (50 dB) as compared to low value of ratio of SI signal after analog-domain cancellation to the desired signal (30 dB). Similarly, Fig. 18 shows the spectral efficiency vs. SNR of IABD 1 in the presence of residual SI for different value of ratio of SI signal after analog-domain cancellation to the desired signal. It is evident from the Fig. 18 that the spectral efficiency performance is better for high value of ratio of SI signal after analog-domain cancellation to the desired signal (50 dB) as compared to low value of ratio of SI signal after analog-domain cancellation to the desired signal (30 dB).

Finally, we compare our proposed method in terms of BER and spectral efficiency with perfect self-interference channel, perfect backhaul channel between IABD 1 and FD enabled IABN, perfect beam alignment and without interference as shown in Fig. 19 and Fig. 20, respectively.

IX. CONCLUSION

In this paper, we evaluate the BER and spectral efficiency performance of multi-cell multi-user large-scale array system with FD enabled IAB network for FR2 band with and without the intra-cell interference in the presence of AWGN. Only RF precoder and combiner are used, and their weights are calculated using set of operations given in beam management. Further, determination of optimum beam index (the beam which gives the highest received signal strength) is also proposed using broadcast channel of 5G NR by extending the SS burst in whole radio frame. The transmission of SS burst in whole radio frame gives better beam alignment between base station and UE due to the increase number of beams. In addition, user selection method based on cross-correlation of RF precoder weights is also proposed which mitigate intra-cell interference. Further, successive interference cancellation is also proposed to mitigate Si in digital-domain SI cancellation. It is evident from simulation results that residual SI limits the BER performance, however the amount of residual SI depends on SIDR. Finally, scheduling algorithm is to performed if the interfering users are in the vicinity of the desired user. In future, we can evaluate the performance of same network with hybrid precoding and in the presence of hardware impairments.

REFERENCES

[1] S. A. Busari, K. M. S. Huq, S. Mumtaz, L. Dai, and J. Rodriguez, "Millimeter-wave massive MIMO communication for future wireless systems: A survey," *IEEE Commun. Surveys Tuts.*, vol. 20, no. 2, pp. 836–869, 2nd Quart., 2018.

[2] T. Zhang, S. Biswas, and T. Ratnarajah, "An analysis on wireless edge caching in in-band full-duplex FR2-IAB networks," *IEEE Access*, vol. 8, pp. 164987–165002, Sep. 2020.

[3] I. A. Hemadeh, K. Satyanarayana, M. El-Hajjar, and L. Hanzo, "Millimeter-wave communications: Physical channel models, design considerations, antenna constructions, and link-budget," *IEEE Commun. Surveys Tuts.*, vol. 20, no. 2, pp. 870–913, 2nd Quart., 2018.

[4] S. Biswas, S. Vuppala, J. Xue, and T. Ratnarajah, "On the performance of relay aided millimeter wave networks," *IEEE J. Sel. Topics Signal Process.*, vol. 10, no. 3, pp. 576–588, Apr. 2016.

[5] M. Polese, M. Giordani, T. Zugno, A. Roy, S. Goyal, D. Castor, and M. Zorzi, "Integrated access and backhaul in 5G mmWave networks: Potential and challenges," *IEEE Commun. Mag.*, vol. 58, no. 3, pp. 62–68, Mar. 2020.

[6] C. Saha and H. S. Dhillon, "Millimeter wave integrated access and backhaul in 5G: Performance analysis and design insights," *IEEE J. Sel. Areas Commun.*, vol. 37, no. 12, pp. 2669–2684, Dec. 2019.

[7] *NR; Study on Integrated Access and Backhaul*, document (3GPP TR 38.874 version 16.0.0 Release 16), 2018.

[8] M. N. Islam, S. Subramanian, and A. Sampath, "Integrated access backhaul in millimeter wave networks," in *Proc. IEEE Wireless Commun. Netw. Conf. (WCNC)*, San Francisco, CA, USA, Mar. 2017, pp. 1–6.

[9] P. Aquilina, A. C. Cirik, and T. Ratnarajah, "Weighted sum rate maximization in full-duplex multi-user multi-cell MIMO networks," *IEEE Trans. Commun.*, vol. 65, no. 4, pp. 1590–1608, Apr. 2017.

[10] A. C. Cirik, S. Biswas, S. Vuppala, and T. Ratnarajah, "Beamforming design for full-duplex MIMO interference channels–QoS and energy-efficiency considerations," *IEEE Trans. Commun.*, vol. 64, no. 11, pp. 4635–4651, Nov. 2016.

[11] M. Jain, J. I. Choi, T. Kim, D. Bharadia, S. Seth, K. Srinivasan, P. Levis, S. Katti, and P. Sinha, "Practical, real-time, full duplex wireless," in *Proc. 17th Annu. Int. Conf. Mobile Comput. Netw. (MobiCom)*, Las Vegas, NV, USA, 2011, pp. 301–312.

[12] A. Sabharwal, P. Schniter, D. Guo, D. W. Bliss, S. Rangarajan, and R. Wichman, "In-band full-duplex wireless: Challenges and opportunities," *IEEE J. Sel. Areas Commun.*, vol. 32, no. 9, pp. 1637–1652, Sep. 2014.

[13] M. Duarte, A. Sabharwal, V. Aggarwal, R. Jana, K. K. Ramakrishnan, C. W. Rice, and N. K. Shankaranarayanan, "Design and characterization of a full-duplex multiantenna system for WiFi networks," *IEEE Trans. Veh. Technol.*, vol. 63, no. 3, pp. 1160–1177, Mar. 2014.

[14] H. Luo, M. Holm, and T. Ratnarajah, "Wideband active analog self-interference cancellation for 5G and beyond full-duplex systems," in *Proc. 54th Asilomar Conf. Signals, Syst. Comput.*, Pacific Grove, CA, USA, Nov. 2020.

[15] E. Ahmed and A. M. Eltawil, "All-digital self-interference cancellation technique for full-duplex systems," *IEEE Trans. Wireless Commun.*, vol. 14, no. 7, pp. 3519–3532, Jul. 2015.

[16] O. Teyeb, A. Muhammad, G. Mildh, E. Dahlman, F. Barac, and B. Makki, "Integrated access backhauled networks," in *Proc. IEEE 90th Veh. Technol. Conf. (VTC-Fall)*, SHonolulu, HI, USA, Sep. 2019, pp. 1–5.

[17] N. Bhushan, J. Li, D. Malladi, R. Gilmore, D. Brenner, A. Damnjanovic, R. Sukhavasi, C. Patel, and S. Geirhofer, "Network densification: The dominant theme for wireless evolution into 5G," *IEEE Commun. Mag.*, vol. 52, no. 2, pp. 82–89, Feb. 2014.

[18] S. Shaboyan, A. S. Behbahani, and A. M. Eltawil, "Practical considerations for full duplex enabled 5G integrated access and backhaul," *J. Signal Process. Syst.*, vol. 92, no. 5, pp. 465–474, Jan. 2020.

[19] J. Zhang, N. Garg, M. Holm, and T. Ratnarajah, "Design of full duplex millimeter-wave integrated access and backhaul networks," *IEEE Wireless Commun.*, vol. 28, no. 1, pp. 60–67, Feb. 2021.

[20] S. Wu, C.-X. Wang, M. M. Alwakeel, and X. You, "A general 3-D non-stationary 5G wireless channel model," *IEEE Trans. Commun.*, vol. 66, no. 7, pp. 3065–3078, Jul. 2018.

[21] I. P. Roberts, H. B. Jain, and S. Vishwanath, "Equipping millimeter-wave full-duplex with analog self-interference cancellation," in *Proc. IEEE Int. Conf. Commun. Workshops (ICC Workshops)*, Dublin, Ireland, Jun. 2020, pp. 1–6.

[22] M. Giordani, M. Polese, A. Roy, D. Castor, and M. Zorzi, "A tutorial on beam management for 3GPP NR at mmWave frequencies," *IEEE Commun. Surveys Tuts.*, vol. 21, no. 1, pp. 173–196, 1st Quart., 2019.

[23] Y.-N.-R. Li, B. Gao, X. Zhang, and K. Huang, "Beam management in millimeter-wave communications for 5G and beyond," *IEEE Access*, vol. 8, pp. 13282–13293, Jan. 2020.

[24] M. Polese, M. Giordani, M. Mezzavilla, S. Rangan, and M. Zorzi, "Improved handover through dual connectivity in 5G mmWave mobile networks," *IEEE J. Sel. Areas Commun.*, vol. 35, no. 9, pp. 2069–2084, Sep. 2017.

[25] *5G NR; Physical Channels and Modulation*, document (3GPP TS 38.211 version 15.3.0 Release 15), 2018.

[26] A. Chakrapani, "On the design details of SS/PBCH, signal generation and PRACH in 5G-NR," *IEEE Access*, vol. 8, pp. 136617–136637, Jul. 2020.

[27] X. Lin, A. Grovlen, K. Werner, J. Li, R. Baldemair, J.-F.-T. Cheng, S. Parkvall, D. C. Larsson, H. Koorapaty, M. Frenne, and S. Falahati, "5G new radio: Unveiling the essentials of the next generation wireless access technology," *IEEE Commun. Standards Mag.*, vol. 3, no. 3, pp. 30–37, Sep. 2019.

[28] T. S. Rappaport and S. Deng, "73 GHz wideband millimeter-wave foliage and ground reflection measurements and models," in *Proc. IEEE Int. Conf. Commun. Workshop (ICCW)*, London, U.K., Jun. 2015, pp. 1238–1243.

A. BISHNU (Member, IEEE) was born in Nowrozabad, India, in 1987. He received the B.E. degree in electronics and communication engineering from the Technocrat Institute of Technology, Bhopal, India, in 2010, the M.E. degree in electronics and telecommunication engineering from SGSITS Indore, India, in 2013, and the Ph.D. degree in electrical engineering from IIT Indore, India, in 2019. In 2019, he was a Visiting Research Scholar with The University of Edinburgh, U.K., where he is currently a Postdoctoral Research Associate. His research interests include channel estimation, cognitive radio, MIMO-OFDM systems, and full-duplex communications. He served as a reviewer for many IEEE and Springer journals.

M. HOLM (Member, IEEE) received the B.S. degree (Hons.) in laser physics and optoelectronics and the Ph.D. degree in physics from the University of Strathclyde, in 1997 and 2001, respectively. He currently works as the Technical Lead and a Hardware System Architect with Huawei Technologies (Sweden) AB, with interest in microwave radio, phased array antennas, full duplex radio systems, and photonic radios. In the past, he was the Microwave Lead on AESA radar systems, a Senior Engineer responsible for GaAs pHemt modeling, and a Laser and Package Design Engineer for SFP/XENPACK fiber modules. He has published in the fields of laser design and GaAs device modeling.

T. RATNARAJAH (Senior Member, IEEE) was the Head of the Institute for Digital Communications, The University of Edinburgh, Edinburgh, U.K., from 2016 to 2018, where he is currently a Professor of digital communications and signal processing. He has supervised 16 Ph.D. students and 21 postdoctoral research fellows, and raised more than $ 11 million USD of research funding. He was the Coordinator of the EU projects ADEL (3.7 M €) in the area of licensed shared access for 5G wireless networks and HARP (4.6 M €) in the area of highly distributed MIMO, and the EU Future and Emerging Technologies projects HIATUS (3.6 M €) in the area of interference alignment and CROWN (3.4 M €) in the area of cognitive radio networks. His research interests include signal processing and information theoretic aspects of beyond 5G wireless networks, full-duplex radio, mmWave communications, random matrices theory, interference alignment, statistical and array signal processing, and quantum information theory. He has published over 400 publications in these areas and holds four U.S. patents. He is a fellow of the Higher Education Academy (FHEA). He was an Associate Editor of IEEE TRANSACTIONS ON SIGNAL PROCESSING, from 2015 to 2017, and the Technical Co-Chair of the 17th IEEE International Workshop on Signal Processing Advances in Wireless Communications, Edinburgh, in July 2016.